

Cite this: DOI: 10.1039/c1ee02073k

www.rsc.org/ees

PAPER

Chemical, ultrastructural and supramolecular analysis of tension wood in *Populus tremula x alba* as a model substrate for reduced recalcitrance†Marcus Foston,^a Christopher A. Hubbell,^a Reichel Samuel,^a Seokwon Jung,^a Hu Fan,^a Shi-You Ding,^b Yining Zeng,^b Sara Jawdy,^c Mark Davis,^b Robert Sykes,^b Erica Gjersing,^b Gerald A. Tuskan,^c Udaya Kalluri^c and Arthur J. Ragauskas^{*a}

Received 4th July 2011, Accepted 2nd September 2011

DOI: 10.1039/c1ee02073k

Biomass is one of the most abundant potential sustainable sources for fuel and material production, however to fully realize this potential an improved understanding of lignocellulosic recalcitrance must be developed. In an effort to appreciate the underlying phenotypic, biochemical and morphological properties associated with the reduced recalcitrance observed in tension stress-induced reaction wood, we report the increased enzymatic sugar yield and corresponding chemical and ultrastructural properties of *Populus* tension wood. *Populus tremula x alba* (PTA) was grown under tension and stem segments containing three different wood types: normal wood (NW), tension wood (TW) from the elongated stem side and opposite wood (OW) from the compressed stem side were collected. A variety of analytical techniques were used to describe changes occurring as a result of the tension stress-induced formation of a gelatinous cell wall layer (G-layer). For example, gel permeation chromatography (GPC) and ¹³C solid-state nuclear magnetic resonance (NMR) revealed that the molecular weight and crystallinity of cellulose in TW is greater than that of cellulose acquired from NW. Whole cell ionic liquid and other solid-state NMR analysis detailed the structure of lignin and hemicellulose in the samples, detecting the presence of variations in lignin and hemicellulose sub-units, linkages and semi-quantitatively estimating the relative amounts of syringyl (S), guaiacyl (G) and *p*-hydroxybenzoate (PB) monolignol units. It was confirmed that TW displayed an increase in PB or H-like lignin and S to G ratio from 1.25 to 1.50 when compared to the NW sample. Scanning electron microscopy (SEM) and coherent anti-Stokes Raman scattering (CARS) were also used to evaluate the morphology and corresponding spatial distribution of the major lignocellulosic components. We found changes in a combination of cell wall properties appear to influence recalcitrance more than any single factor alone.

^aBioEnergy Science Center, School of Chemistry and Biochemistry, Institute of Paper Science and Technology, Georgia Institute of Technology, 500 10th St., Atlanta, GA, 30332, USA. E-mail: Art.Ragauskas@chemistry.gatech.edu; Fax: +1-404-894-4778; Tel: +1-404-894-9701

^bBioEnergy Science Center, National Renewable Energy Laboratory, Golden, CO, 80401

^cBioEnergy Science Center, Oak Ridge National Lab, Oak Ridge, TN, 37831

† Electronic supplementary information (ESI) available. See DOI: 10.1039/c1ee02073k

Broader context

Presently several species of *Populus* are being considered as high potential energy crops because they exhibit drought tolerance, resistance to pests and insects, and the ability to produce high biomass yields on range of lands. More importantly, the relatively compact genome size (40 times smaller pine) and extensive sequencing of the *Populus* genome has made it possible to enhance many of these characteristics unlike ever before through genetic modification. However before researchers can rationally target genes to generate the next generation of transgenics to increase biomass-to-bioethanol production, key phenotypic and genotypic data must be linked to recalcitrance related substrate characteristics. Tension wood has been studied before as a model substrate, however no study comprehensively correlates observed reduce recalcitrance with the wide array of morphological, ultrastructural and chemical properties as done in this study. Ultimately these results will be used to extend the insights on mechanisms of recalcitrance and how those insights could be used to engineer reduced recalcitrance to saccharification.

Introduction

Tension wood (TW) is a form of reaction wood formed as part of a corrective growth mechanism in response to longitudinal tensile growth stress in woody angiosperm stems.^{1–3} In some hardwoods, such as *Populus*, TW is characterized by the formation of an additional secondary wall layer at the interior side of the xylem fibers. This layer appears as a thick, translucent, gelatinous ring which has been named the G-layer.² This G-layer has many important ultrastructural modifications with respect to a typical secondary wall structure, mainly related to its composition, which is almost entirely cellulose.² Additionally, TW is characterized by relatively higher cellulose and lower lignin levels and increased number of xylem fiber cells and more secondary wall material (biomass), all of which contribute to desirable characteristics of feedstock materials for bioethanol production. Understanding the underlying phenotypic, biochemical and morphological properties of model biomass such as *Populus* TW are central to informing the design of suitably tailored feedstocks.

The majority of data on TW is related to the change in the distribution of cell wall chemical composition. Lignin staining experiments using safranin light green and phloroglucionol-HCl indicate the presence of a non-lignified ultrastructure in the G-layer of *Populus*, whereas other cell wall layers external to the G-layer showed heavy staining suggesting a strongly lignified composition.² The distribution of substructure and composition of TW have also been studied by X-ray photoelectron spectroscopy (XPS), analyzing the C 1s and O 1s spectra for binding energies of various functional groups such as C–OH attributed to cellulose/hemicellulose and C–(C, H) primarily attributed to lignin. Using XPS, samples from the pith, bark and the in between regions of greenhouse grown aspen plants were analyzed before and after inducing TW formation.⁴ The changes in molecular concentration of functional groups observed in the C 1s and O1s spectra suggested that a lower lignin and higher cellulose/hemicellulose content exist in living aspen TW.

Similarly, ultraviolet (UV) microspectrophotometry has been used to not only confirm lower lignin contents in the G-layer but also to demonstrate a shift in lignin distribution. Monitoring different absorption maxima it was determined that lignin content decreased and the estimated syringyl/guaiacyl ratio increased with increasing tensile strain during *Populus* cell wall growth.⁵ Imaging experiments with *Populus* and antibodies specific for guaiacyl and syringyl lignin epitopes were used to image the tension wood samples by immunogold electron microscopy. The resulting micrographs estimate a 40% increase in the relative abundance of S monolignol units into the G-layer with respect to the S2 wall layer.^{2,6}

There have also been a few studies looking at the ultrastructure of cellulose in the G-layer of *Populus* and *Betula* using electron microscopy. These results suggest that cellulose in the G-layer is arranged in a highly crystalline form with microfibrils oriented nearly parallel to the longitudinal axis. Field emission scanning electron microscopy (FE-SEM) was used on crystalline cellulose in *Populus* TW labeled *via* conjugation to a cloned carbohydrate-binding module with linkages to gold/silver nanoparticles for imaging by electrons. The FE-SEM images confirm that the cellulose microfibrils in the G-layer are well-defined, concentri-

cally oriented aggregates on the order of 30–40 nm with a microfibril angle of almost 0°. X-ray diffraction studies of single TW fibers not only indicated an increased crystallinity and reduced microfibril angle, but showed an almost four-fold increase in crystallite cross-sectional dimensions when compared to the S2 wall layer.^{1,3,7}

Enzymatic hydrolysis of lignocellulosic substrates has been studied for sometime to determine the potential effect of substrate characteristics, such as crystallinity, degree of polymerization (DP), specific surface area, and lignin distribution on the ease of cellulose deconstruction by cellulase.⁸ However, the relationship between substrate characteristics and enzymatic hydrolysis is a complex, multivariate issue, and while many studies have attempted to simplify this problem by manipulating individual properties, the processes used which can alter a single substrate property invariably change a variety of substrate properties. Typically, chemical/mechanical treatments, and more recently genetic engineering, have been employed to alter substrate characteristics in an attempt to deconvolute the effects of substrate chemistry, structure and morphology, on the fundamental nature of recalcitrance and to improve the processability of agro-energy crops.⁹ This investigation is one of the few examples which utilize an enzymatic sugar assay to evaluate the recalcitrance of tension stress-induced reaction wood while also characterizing this model feedstock by a number of advanced techniques, providing a comprehensive and detailed analysis of the chemical and ultrastructural features known to affect biomass recalcitrance.

There have been limited studies utilizing solid-state and liquid NMR, GPC, py-MBMS or confocal-Raman microscopy¹⁰ to characterize the ultrastructure of cellulose and the chemical/spatial profile of lignin in tension wood fibers. A key prior study, reported by Horii *et al.* in which proton spectral editing of ¹³C CP/MAS NMR was used to isolate the spectrum of crystalline cellulose, determined that for *Populus maximowiczii* tension wood, cellulose I_β was the dominant crystalline allomorph.³ In this study, we present the use of solids and liquid NMR techniques in novel combination with other analytical and imaging techniques to probe the fundamental ultrastructure of tension and normal wood in *Populus tremula x alba* (PTA) as a means of evaluating the changes occurring during tensile stress-induced growth. We also conducted enzymatic hydrolysis experiments on PTA grown under tension and normal growth condition in an effort to assess the change in the recalcitrance of the tension stress-induced reaction wood. The goal of the present study is to investigate the lignocellulosic chemistry and ultrastructural properties of tension stress-induced reaction wood as they relate to sugar release efficiency or recalcitrance properties of biomass.

Results and discussion

The reduced lignin content levels, altered carbohydrate and lignin structures, and different cell wall layer organization in *Populus tremula x alba* (PTA) tension wood could provide a reactive substrate for enzymatic deconstruction. Studying model substrates such as this are especially relevant to improved biofuel production in light of recent publications that demonstrate that plant recalcitrance is reduced as lignin levels and the ratio of S to G monolignols in tobacco, alfalfa and switchgrass

are genetically modified.¹¹ Enzymatic hydrolysis of lignocelluloses is influenced by biomass recalcitrance which in turn is affected by various substrate characteristics including cellulose crystallinity, degree of polymerization, accessibility of surface area, lignin and hemicellulose distributions. Therefore, in an effort to evaluate the altered recalcitrance of tension stress-induced reaction wood, a critical analysis is the assessment of the enzymatic response to tension wood (TW). The PTA normal wood (NW) and opposite wood (OW) samples generated for this study showed little response to cellulase (Fig. 1), yielding ~7–9% sugar release after 48 h treatment. However, the TW sample demonstrated a remarkable 3-fold increase in cell wall digestibility with respect to the NW and OW samples. This increase in cell wall digestibility is of course in part due to the up-regulation of cellulose accumulation in the G-layer, although as shown later is much higher than the increase in relative glucose content. This suggests at least one other substrate factor has led to this change in recalcitrance. To examine this enhanced cellulase reactivity, the cell wall chemistry and ultrastructure of these wood samples were examined in depth.

Imaging

Scanning electron microscopy (SEM) images of cross-sections from NW, TW and OW stems were taken under two different magnifications (Fig. 2). The images at a resolution of 20 μm (Fig. 2a–2c) clearly show differences in the organization of vessel elements and relative amount of cell wall material per volume. When compared to the NW and OW samples, the TW sample displays significantly more cell wall material with an increased number of xylem fiber cells and vessels of smaller diameter. Upon higher magnification, further differences are observed showing a much thicker cell wall with G-layer formation in the TW sample denoted by the red arrow. Based on these images, the available specific surface area in the cell wall and relative amount of cellulosic material per unit volume seems to be significantly increased in the tension wood. For tension wood, sugar release efficiency has not typically been correlated with changes in chemical/ultrastructural features, however an increase in the availability of cellulose at the plant cell level has been proposed to be beneficial for enzymatic deconstruction^{8,12–15} and is consistent with the observed enhancement in glucose release (Fig. 1).

A cutting edge chemical imaging technique was applied to explore the location of cell wall lignin in the control and tension

PTA samples, cross-sections were imaged using coherent anti-Stokes Raman scattering (CARS). The Raman vibrational mode at 1,600 cm^{-1} has been attributed to the symmetric aromatic ring C=C stretching of lignin and this spectral signal has been used to image lignin distribution in the plant cell.^{16,17} Like traditional Raman imaging, contrast is based on molecular vibrations, however, CARS is a non-linear process utilizing two laser light sources to generate anti-Stokes signals. When tuned properly to match a particular Raman-active vibrational frequency, the resulting coherent signal is orders of magnitude greater than that from spontaneous Raman scattering providing sufficient intensity to image complex structures such as the cell wall.^{16,17}

CARS images of the PTA NW, OW and TW samples (Fig. 3b–e) were taken at different positions across the tension sample stem, avoiding the pith, with locations denoted in autofluorescence images of the tension sample stem (Fig. 3a). The NW image (Fig. 3b) shows a very uneven distribution of lignin across the cell walls, with the middle lamella and cell corners having the greatest lignin content. The OW displays a similar lignin distribution to the control with an even more heterogeneous lignin spatial distribution particularly in the transition areas of the secondary cell wall layers. The image in Fig. 3c was taken on the tension stem side just past the pith, and clearly indicates a thickening of the secondary cell wall. The final image of the tension stress-induced reaction wood in Fig. 3d shows the thick G-layer in the secondary cell wall which is physically separated from the S1 and S2 cell wall layers. With the addition of the G-layer to the secondary cell wall of the tension wood the image in Fig. 3d suggests that the relative lignin content in the TW sample, when compared to the secondary cell wall of the NW sample is lower. However, the image of the tension wood indicated that the S1 and S2 cell wall layers, compound middle lamella and cell corners contain lignin.

Carbohydrate and lignin distribution

The chemical composition of tension wood, more specifically the G-layer has been of interest since the early 1970's,^{2,18} mainly related to the distribution of lignin and cellulose in tension woods, using techniques such as, microscopy of selectively stained samples and UV microspectrophotometry. The general consensus of these studies is that there is a decrease in lignin content in tension wood accompanied by an increase in the S/G ratio in the secondary cell wall. Work studying hemicellulose in tension wood of *Betula verrucosa*, showed an increase in the relative amount of glucose by ~10% and a statistically significant decrease in xylose and mannose contents with respect to the tension stem face.¹⁸

In our study, HPLC based anion-exchange chromatography was performed on acid hydrolyzed stem segment samples from PTA grown under normal and tension conditions. Fig. 4 summarizes the variation in carbohydrate, including contents of the major hemicellulose sugars such as xylose, mannose, arabinose, and galactose and Klason lignin distribution due to tension stress-induced reaction wood formation. In an effort to further probe the chemical structures constituting the cell wall of tension wood, pyrolysis molecular beam mass spectrometry (py-MBMS) was performed on stem segment samples from PTA. The intensity of characteristic cell wall polymer mass fragments in the

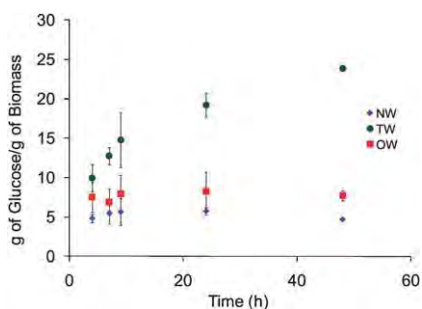


Fig. 1 Enzymatic sugar release *Populus tremula x alba* (PTA) samples grown under tension and normal conditions. Error bars represent the standard deviation of two trials.

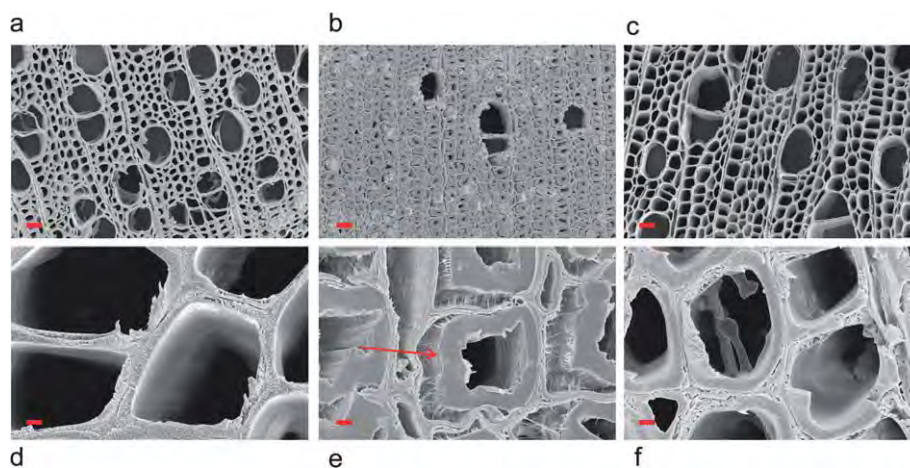


Fig. 2 Electron micrograph of cross-sectioned *Populus tremula x alba* (PTA) stems grown under bending or normal (erect) conditions. (a–c) red scale bar represents 20 μm and (d–f) red scale bar represents 2 μm . The red arrow denote the G-layer formation. (a,d) NW; (b,e) TW and (c,f) OW.

py-MBMS spectra were calibrated against a large set of standard biomass samples with known lignin contents. This calibration curve was in turn used to determine the relative % of lignin in the TW, OW and NW samples, generating statistically insignificant differences in lignin results to the wet chemistry determined Klason lignin contents ($24 \pm 2\%$, $27 \pm 2\%$ and $27 \pm 2\%$, respectively). Based on the age of the PTA cutting, assuming consistent longitudinal sectioning with respect to the ratio of sampled normal and reaction wood cells and the amount of time the stem was grown under tension, a rough estimate indicates that the TW and OW samples have a maximum of $\sim 33\%$ reaction wood. Utilizing this estimate for the percentage of reaction wood and the above carbohydrate distribution in the TW

sample, one may expect the lignin and xylan contents within the reaction wood cell to be as low as $\sim 7\%$ and 5% , respectively.

The most significant finding seems to be that the $\sim 25\%$ increase in the amount of available glucose in the TW sample resulted in a $\sim 300\%$ increase in cellulase sugar release in comparison to the NW or OW enzymatic hydrolysis experiments. This increase in sugar yield becomes even more impressive taking into consideration all samples contained less than 2% starch by dry weight of biomass determined by a published HPLC procedure utilizing an amylase treatment.¹⁹ Considering the differences in the magnitude of increase, this change in digestibility profile cannot be simply related to the increase of glucan content, but instead is more than likely attributed, in part,

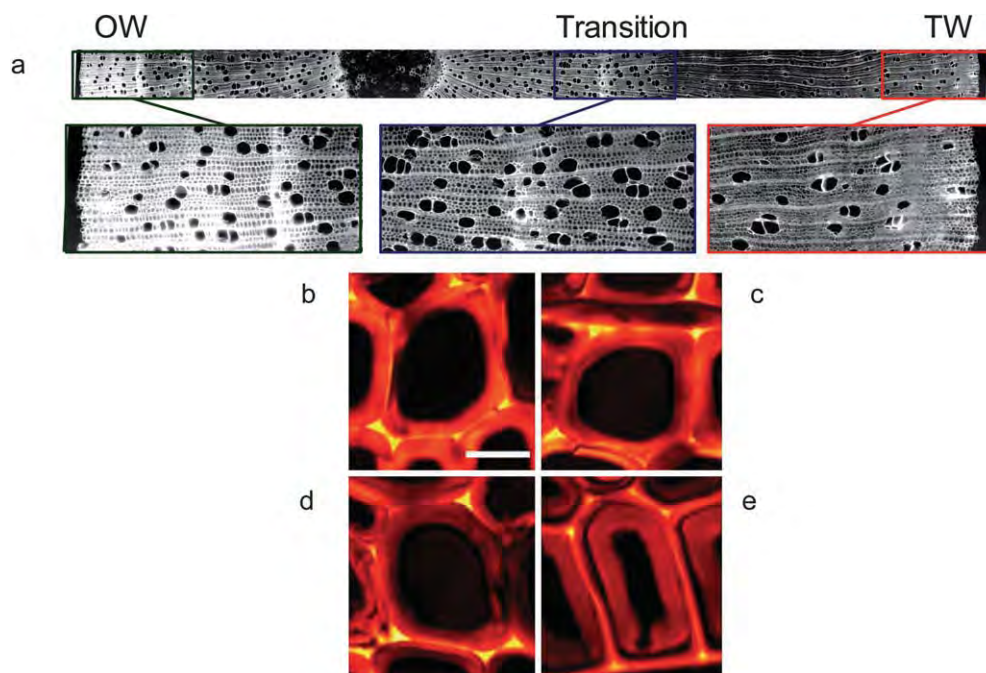


Fig. 3 (a) Autofluorescence and (b–e) chemical imaging of cross-sectioned *Populus tremula x alba* (PTA) stems grown under bending or normal (erect) conditions using CARS microscopy, white scale bar represents 10 μm and yellow indicates areas of high lignin content. (b) NW; (c) OW; (d) transition area between OW and TW; (e) TW.

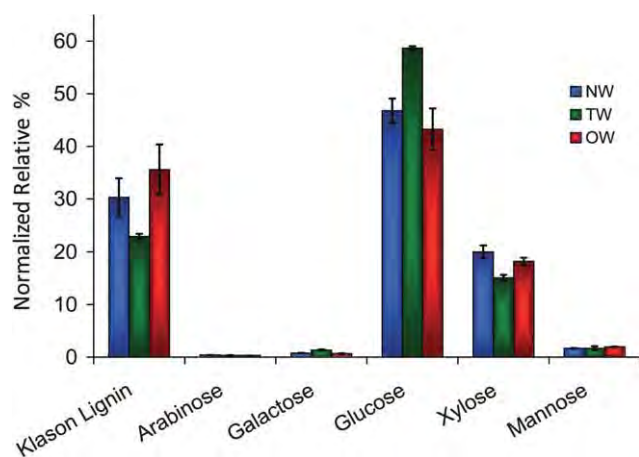


Fig. 4 Carbohydrate and Klason lignin distribution of *Populus tremula x alba* (PTA) samples grown under bending or normal (erect) conditions as determined by HPLC and normalized by the sum of all the measured components. Error bars represent the standard deviation of two trials.

to some other combination of differences within the cell wall structure of tension wood.

Gel permeation chromatography

The ratio of terminal to interior β -glucosidic bonds is determined by the degree of polymerization (DP) of cellulosic substrates which can be significant and potentially rate-determining with respect to the activity of exo cellulases.¹⁵ It is, therefore, important to understand and deconvolute the role that cellulose DP has in biomass recalcitrance. A potential route to do this is by studying the change in the molecular weight of cellulose within the G-layer of tension wood with respect to the observed changes in enzymatic hydrolysis (Fig. 1).

The average degree of polymerization of isocyanate derivatized α -cellulose isolated from PTA samples grown under tension and normal conditions as determined by integration of GPC chromatographs were plotted (Fig. 5). The data clearly shows that cellulose in the TW samples for PTA have larger average molecular weights than the NW or OW samples. This result is particularly informative, because one of the major substrate characteristics linked to recalcitrance is the relative number of cellulosic reducing ends and/or cellulose DP.²⁰ The DP of cellulose in the TW samples was the highest, yet those samples seemed to be the least recalcitrant, suggesting DP of cellulose is most likely not the main determinant in the enzymatic degradation of TW *versus* OW and NW cellulose. However, it should be noted that that cell wall cross-linkages were not studied here and could be important to sugar release efficiency.

Solid-state NMR

Using ¹³C CP/MAS NMR and a 2-peak integration analysis²¹ of the C₄ region in the acquired spectrum of PTA (Supplementary Fig. S2†), crystallinity data was calculated and tabulated in Table 1. The TW sample displayed the highest crystallinity, and this is consistent with reported X-ray diffraction results of single tension-wood fibers from *Populus* which show nearly perfect crystalline cellulose microfibrils in the G-layer.⁷ Using the

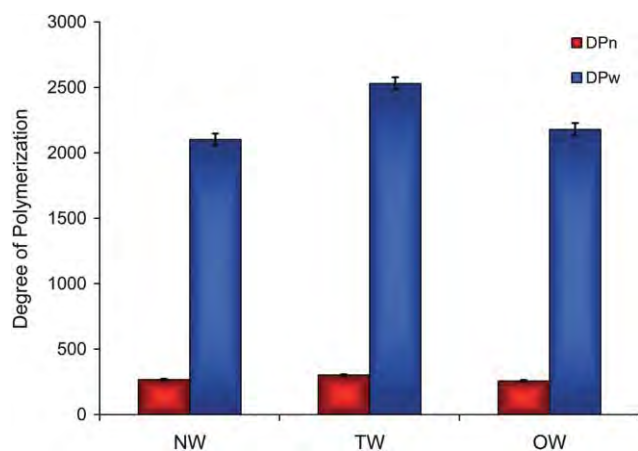


Fig. 5 Number- and weight-average degree of polymerization of NaOH isolated α -cellulose from *Populus tremula x alba* (PTA) samples grown under bending or normal (erect) conditions as determined by integration of the GPC chromatographs. Error bars represent the standard deviation of two trials.

crystallinity of the NW sample as a baseline and the fact the TW sample may have as much as $\sim 33\%$ reaction wood, a weighted average calculation suggest the crystalline content of the G-layer of TW to be as high as $\sim 65\%$. It has been postulated that crystalline regions reduce the resulting enzymatic degradation of cellulose,^{8,14,15} yet the cellulose crystallinity in the TW samples was the highest. However, the TW samples displayed significant increases in the extent of enzymatic saccharification suggesting cellulose crystallinity alone may not be the critical determinant in the enzymatic degradability of TW cellulose.

A 7-peak non-linear line-fit analysis^{22,23} on the C₄ region was also performed to determine the relative amounts of crystalline allomorphs present. The OW and NW samples contained similar proportions of cellulose I _{α} and I _{β} , whereas like the aforementioned study by Horii *et al.*, the results for the TW sample seemed to indicate cellulose I _{β} was the dominant crystalline allomorph in the tension stress-induced reaction wood of PTA.

Lateral fibril (LFD) and lateral fibril aggregate (LFAD) dimensions can be estimated using the relative intensity of peaks attributed to total fibril surfaces and accessible fibril surfaces.²⁴ Based on those intensities and a square cross-sectional microfibril model comprised of chains having a width of 0.55 nm, the LFD and LFAD were estimated for the normal, tension and opposite PTA stem segment samples (Table 1). The results indicate the TW samples on average show larger LFD and

Table 1 % Crystallinity, lateral fibril dimension and lateral aggregate fibril dimension for *Populus tremula x alba* (PTA) samples grown under bending or normal (erect) conditions as a result of integration and non-linear line-fits of ¹³C CP/MAS spectra. Standard deviations are based on two trials

Sample	CrI %		LFD (nm)		LFAD (nm)	
	Avg	Stdev	Avg	Stdev	Avg	Stdev
NW	53	1	3.7	0.2	17.9	3.2
TW	57	1	4.5	0.1	21.5	2.0
OW	52	3	3.9	0.3	20.9	1.2

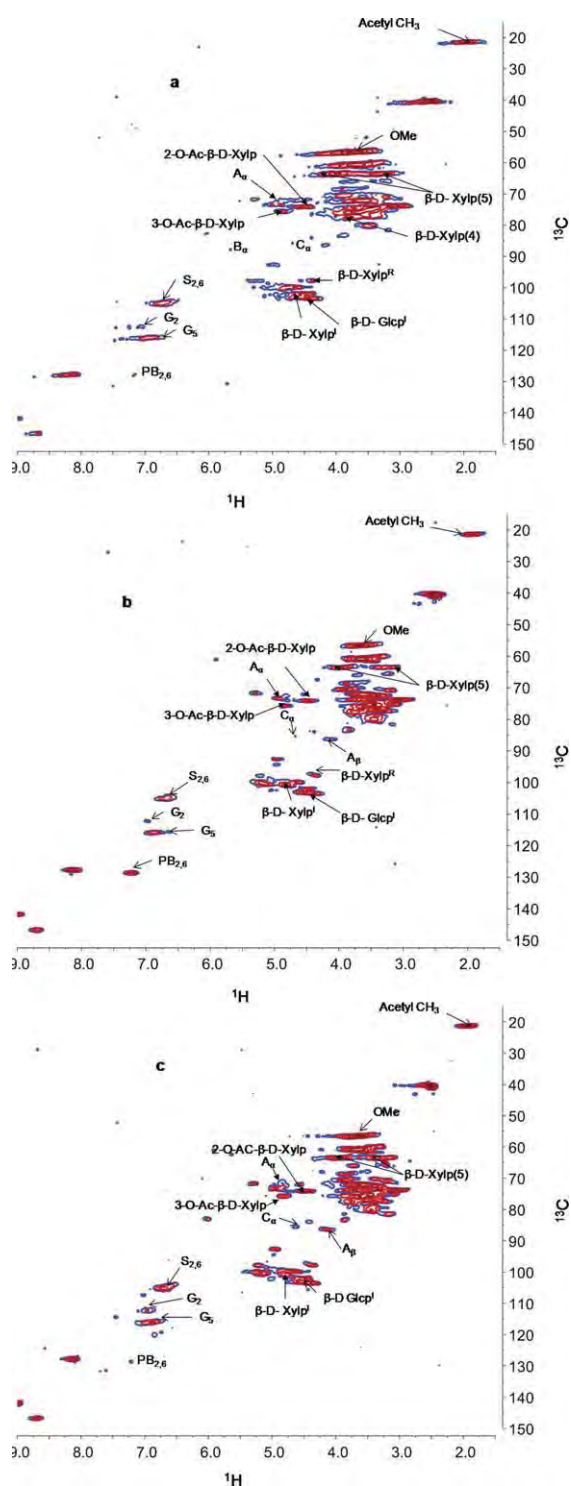


Fig. 6 Whole plant cell wall 2D ^{13}C - ^1H heteronuclear single quantum correlation (HSQC) NMR spectra of *Populus tremula x alba* (PTA) samples grown under bending conditions in an ionic liquid/DMSO mixture. (a) NW; (b) TW; (c) OW. 2-O-Ac- β -D-Xylp: C_2/H_2 correlation for the acetylated β -D-xylopyranoside units; 3-O-Ac- β -D-Xylp: C_3/H_3 correlation for the acetylated β -D-xylopyranoside units; A: β -aryl ether linkage; B: phenylcoumaran; C: resinol; β -D-glucp^I: Internal β -D-glucopyranoside units; β -D-Xylp^I: Internal xylopyranoside units; S: syringyl; G: guaiacyl; PB: *p*-hydroxybenzoate; Cross-peaks at $\delta_{127.5/8.14}$, $146.4/8.69$, $141.4/9.05$ are from pyridinium chloride.

similar LFAD values with respect to either the NW or OW samples. Referring to the literature, XRD results on tension-wood fibers show a four-fold increase in the crystalline dimensions of the G-layer when compared to those measured in the S2 layer.⁷ This was attributed to either a different biosynthetic deposition of cellulose in the G-layer or increased aggregation of cellulose chains due to a reduced lignin and hemicellulose content. The later point could be significant with respect to increased enzymatic degradation and reduced recalcitrance particularly since hemicellulose and lignin removal *via* pretreatment has been cited as a key issue in increased sugar yields.²⁵⁻²⁷

^1H - ^{13}C HSQC ionic liquid NMR

Lignin has been shown to limit the use of biomass in biofuel energy production, therefore strategies of lignin down-regulation have become of considerable interest.^{28,29} The generation of tension wood involves both the natural down-regulation of lignin and increased accumulation of cellulose within localized zones. ^1H - ^{13}C HSQC ionic liquid NMR can be a particularly useful tool to better understand the natural alteration of lignin during the formation of tension stress-induced reaction wood and how it may affect enzymatic degradation of cellulose.

The PTA whole cell correlation spectra (Fig. 6) exhibited prominent cross peaks for C_2 - C_6 in polysaccharide units along with overlapping lignin side chain units in the region of $\delta_{\text{C}}/\delta_{\text{H}}$ 56.0–82.0/3.0–4.1 ppm.³⁰⁻³² Other major correlations appeared for C_2 -acetylated (2-O-Ac- β -D-Xylp) and C_3 -acetylated xylan (3-O-Ac- β -D-Xylp) at $\delta_{\text{C}}/\delta_{\text{H}}$ 74.0/4.5 (C_2/H_2) and 75.0/4.8 (C_3/H_3) ppm, respectively.³⁰⁻³² The function, biosynthesis and reduction/removal of cell wall hemicellulose and lignin seem invariably linked and therefore understanding changes in hemicellulose acetylation pattern due to tension stress-induced reaction wood formation is vital. Based on the relative integration of these resonances, the ratio of C_2 -acetylated xylan *versus* C_3 -acetylated xylan was determined and reported in Table 2. In the NW sample the ratio of C_2 -acetylated xylopyranoside: C_3 -acetylated xylopyranoside was $\sim 1:1$ increasing to 1.8:1 and 2.1:1 for the TW and OW samples, respectively. In the polysaccharide anomeric region ($\delta_{\text{C}}/\delta_{\text{H}}$ 90.0–105.0/4.4–5.5 ppm) the signals were fairly well resolved.³⁰⁻³² The partial characterization of glucan (cellulose) and xylan (hemicellulose) was accomplished by the cross peaks for internal anomeric signals of the (1–4) linked β -D-glucopyranoside (β -D-glucop^I) at $\delta_{\text{C}}/\delta_{\text{H}}$ 102.8/4.4 ppm and (1–4) linked β -D-xylopyranoside (β -D-xylp^I) at 102.4/4.6 ppm respectively.³⁰⁻³²

The major lignin inter-unit observed in Fig. 6 was the β -aryl ether linkage (A), however traces of phenyl coumaran (B) and resinol (C) were characterized from the C_α -H correlations at $\delta_{\text{C}}/\delta_{\text{H}}$ 71.8/4.8 (A_α), 87.5/5.6 (B_α) and 85.7/4.6 (C_α) ppm respectively for the PTA NW sample.³⁰⁻³² A dominant ^{13}C - ^1H lignin correlation due to methoxyl groups was observed at $\delta_{\text{C}}/\delta_{\text{H}}$ 55.7/3.8 ppm.³⁰⁻³² The spectra for the TW sample indicate a qualitative decrease in the proportion of β -aryl ether linkages and slight increase in resinol sub-structures with respect to the NW sample. The OW spectra also displayed a decrease in β -aryl ether and an increase in resinol linkages. Phenyl coumaran sub-structures were not detected for the TW and OW samples. The presence of aromatic lignin units syringyl (S), guaiacyl (G) and *p*-hydroxy

Table 2 Major structural differences observed by NMR spectra and py-MBMS of *Populus tremula x alba* (PTA) samples grown under bending or normal (erect) conditions in an ionic liquid/DMSO mixture

	2-O-Ac: 3-O-Ac	PB _{Sample} :PB _{NW}	S:G by CP/MAS	S:G by py-MBMS
NW	1.0 : 1.0	1	1.25	1.4
TW	1.8 : 1.0	4	1.50	1.5
OW	2.1 : 1.0	1	1.25	1.4

phenyl-type or *p*-hydroxybenzoate (PB) units were confirmed by the separate contour for S_{2,6}, G₂, and PB_{2,6} at $\delta\text{c}/\delta\text{H}$ 103.8/6.6 (S_{2,6}), 111.0/7.0 (G₂), 128.0/7.2 (PB_{2,6}) ppm, respectively.^{30–32} From the relative volume integration of PB_{2,6} cross-peaks the relative change in H-like monolignol units was semi-quantitatively determined and is also summarized in Table 2.

A qualitative assessment of cross-peak intensity along with the results in Table 2 demonstrate a significant increase in PB lignin, by a factor of 4, and a corresponding decrease in G lignin for the TW sample with respect to NW or OW. The PB lignin content in OW was very similar to NW. In the case of S lignin, a noticeable decrease was observed in the TW sample which was accompanied by decreased peak intensity of β -aryl ether linkages and methoxyl groups. Apparently, the G units decrease was predominant, which could be the reason for the increase in S/G ratio of TW. Due to the semi-quantitative nature of correlation NMR and the significantly reduced signal-to-noise for lignin related resonances in the TW spectra resulting from reduced lignin contents, ¹³C CP/MAS was performed to quantitatively determine S/G ratios (Table 2 and Supplementary Fig. S3†). This was accomplished by spectral subtraction of a pine wood spectrum, which contains only G lignin and by determining S and G lignin contributions to the NW, TW and OW spectra following a published procedure.³³ These results are consistent with work highlighted in a review of lignification and tension wood by Pilate *et al.*, who reported an overall decrease in lignin content in tension wood and an increase in S/G ratio when comparing normal wood and opposite wood *via* histological staining and UV microspectrophotometry.² Similarly, Jin *et al.* studied the tension wood properties of yellow *Populus* and found higher S/G ratio with tensile growth strain and lower S/G ratio with mostly compressive growth strain by histochemical staining and expression analysis.³⁴ This finding could be significant as results from enzymatic hydrolysis have confirmed an increase in sugar release for down-regulated C3H

or HCT transgenic alfalfa lines.²⁸ These transgenic plants had lower total lignin with altered S/G ratios when compared to the wild-type plants.^{28,35} These results are consistent with literature reports that a decrease in lignin content leads to a less recalcitrant biomass.²⁸

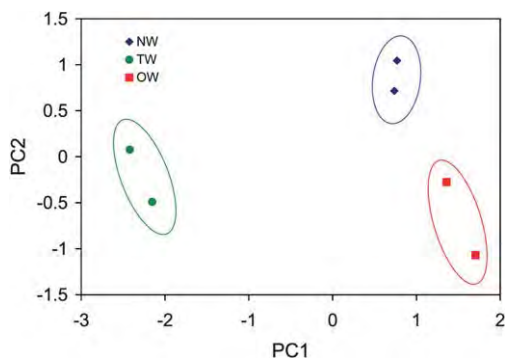
Pyrolysis molecular beam mass spectrometry

In an effort to further extract chemical information from the TW sample and complement NMR determinations of S/G ratios (Table 2), py-MBMS data was analyzed focusing on fragments attributed to monolignol units along with the complete mass fragment spectra. One particularly beneficial feature of py-MBMS analysis is that, regardless of whether the origin of the mass fragments has been identified or not, principal component analysis (PCA) of the mass fragmentation spectra can be used to group samples based on their chemical similarities and differences. For example, PCA of py-MBMS data allowed Kelley *et al.* to distinguish between native coconut, palm, kenaf, and flax samples, and kenaf samples treated in different ways based on the spatial grouping in the principal component plot resulting from PCA.³⁶ Similarly, NW, TW and OW formed distinct groups (outlined as oval groups in the principle component plot in Fig. 7), clearly indicating that the cell wall chemistry has considerable variation which is consistent with the data seen in the ¹H-¹³C HSQC NMR and wet chemistry carbohydrate/lignin analysis.

Conclusions

The results of the present study clearly demonstrate the usefulness of CARS, ¹³C CP/MAS, py-MBMS and GPC as tools to analyze tension wood. ¹³C CP/MAS and integration of the cellulose C₄ region of cellulose from *P. tremula x alba* grown under tension show the crystallinity in the TW sample is higher than in the OW or NW samples. Based on the crystallinity of the normal samples as a baseline and that ~33% of the cell wall material consists of G-layer formations, the extrapolated crystallinity in those regions were determined to be about 65%. Not only did the TW samples exhibit higher % crystallinity, the % total and accessible fibril surfaces suggests that the cellulose microfibril dimensions are larger in tension wood than normal wood. This was correlated to the higher relative glucose and lower relative xylose and lignin contents as determined by HPLC carbohydrate and Klason analysis in the tension wood sample when compared to the normal wood samples. The molecular weight of cellulose in the G-layer of tension wood was higher than normal wood and this was accompanied by changes in the PB:G:S ratio (*p*-hydroxybenzoate is a *p*-hydroxy phenyl-type monolignol unit found in *Populus*).

Based upon the increased enzymatic glucose release seen in Fig. 1 and the various other observations generated by a variety

**Fig. 7** Results of the principal component analysis of py-MBMS data *Populus tremula x alba* (PTA) samples grown under bending or normal (erect) conditions.

of complementary techniques, the G-layer of tension wood from *Populus* could become an attractive bioresource for the biological conversion of cellulosic feedstock to biofuels. Moreover, the unique substrate alterations occurring as a result of tension stress-induced reaction wood formation suggest cellulose crystallinity and DP considered as isolated factors may not be as significant to recalcitrance as once thought. Instead, the results of this study seem to indicate some combination of increased accessible specific surface area, localized lignin down-regulation and chemical alteration along with increased accumulation of cellulose considerably increases enzymatic hydrolysis yields and reduces biomass recalcitrance.

Methods

Substrates

Populus tremula x *alba* (PTA) clonal cuttings were grown for six months in total and pooled stem segments were collected from normal unstressed stems (NW), stems under tension on the elongated side (TW) or stems under tension on the compressed side (OW). TW specifically refers to the wood containing a G-layer, while the wood between TW and OW (pith) is excluded from ground samples in an effort not to obscure further analysis. Tension was applied by fixing each stem at a 90° angle, as shown in Fig. 8, for ~one third of the total stem age or 60 days prior to removing stem segments. All stem material was debarked and elongated/compressed side longitudinal sections were cut manually along the entire length of the stem avoiding the pith. Extractives were subsequently removed from both ground and sectioned samples by placing the biomass into an extraction thimble in a Soxhlet extraction apparatus. The extraction flask was filled with 1 : 2 ethanol:benzene mixture (~150 mL) and then refluxed at a boiling rate which cycled the biomass for at least 24 extractions over a 4 h period.

Ground *Populus* stem

The biomass was sized-reduced in a Wiley mill using 20–80 mesh screens. The milled sample was stored at –20 °C for further treatment.

Cryotome section of *Populus* stem

Cryotome section of *Populus* was accomplished by employing a slight modification of a published literature method.³⁷ In brief, a piece of *Populus* stem less than 2 cm in diameter was sectioned to 50 µm thickness using a LEICA CM 3050S cryostat equipped with a disposable steel blade and embedding material (OCT compound, Tissue-TEK). Disposable steel blades were installed and used after removing the lubricant on the blade surface using dichloromethane and ethanol. To avoid any contamination from the embedding material, a piece of *Populus* stem was attached on the metal plate using a small amount of glue on the bottom edge instead of embedment. The chamber temperature for cryotome section was adjusted at –8 °C and cutting speed was manually controlled. Wood samples were cross sectioned to 50 µm thickness. The cross sections of *Populus* stem were stored between glass slides at –20 °C in freezer to prevent rolling up and to maintain their native forms.



Fig. 8 Photographs of *Populus tremula* x *alba* (PTA) clonal cuttings grown under bending conditions.

Enzymatic hydrolysis

Cellulase (4-glucano-hydrolase) from *Trichoderma reesei* ATCC 26921 and Novozyme 188 (cellobiase) from *Aspergillus niger* were purchased from Aldrich–Sigma and used as received. The activities of cellulase and cellobiase were determined to be 91.03 FPU/ml and 387.70 CBU/ml respectively according to the literature procedures.³⁸ The pulp (0.200 g) was suspended in 50.00 mM citrate buffer adjusted to pH 4.8 by sodium hydroxide at a consistency of 1% (w/v). These two enzymes were added into the suspension at enzyme loading of 20 FPU/g and 40 CBU/g respectively. The mixture was incubated at 50 °C under continuous agitation at 150 rpm. 0.10 mL liquid hydrolysis samples at time intervals of 4, 7, 9, 24 and 48 h were withdrawn and the hydrolysis was quenched by submersion for 5 min in a vigorously boiling water bath. The liquid samples were then diluted to 1.00 mL and were stored at –20 °C until analysis on an Agilent GPC SECurity 1200 system equipped with an acidic ion-exchange column (Bio-Rad HPX-871) and Agilent refractive index (RI) detector using a 10 mM nitric acid solution as the mobile phase (1.0 mL/min) with injection volumes of 20 µL, performed similar to literature procedures.³⁹

Carbohydrate and acid-insoluble lignin (Klason lignin) analysis

Samples for carbohydrate constituents and acid-insoluble lignin (Klason lignin) analysis of both sectioned and ground *Populus* were prepared using a two-stage acid hydrolysis protocol based on TAPPI methods T-222 om-88 with a slight modification. The first stage utilizes a severe pH and a low reaction temperature (72 vol. % H₂SO₄ at 30 °C for 1 h). The second stage is performed at much lower acid concentration and higher temperature (3 vol. % H₂SO₄ at 121 °C for 1 h) in an autoclave. The resulting solution was cooled to room temperature and filtered using G8 glass fiber filter (Fisher Scientific, USA). The remaining residue which is considered as Klason lignin was oven-dried and weighed to obtain the Klason lignin content. The filtered solution was analyzed for carbohydrate constituents of the hydrolyzed *Populus* samples determined by

high-performance anion-exchange chromatography with pulsed amperometric detection (HPAEC-PAD) using Dionex ICS-3000 (Dionex Corp., USA).⁴⁰ Error analysis was conducted by performing carbohydrate and acid-insoluble lignin analysis at least twice on ground samples. The plotted data represent the average and the error bars are one standard deviation.

Optical and scanning electron microscopy (SEM)

Autofluorescence images of cross-sectioned samples were taken by a normal fluorescence microscope using an Olympus IX71 with DP70 camera and 20x lens. All cross-sectioned samples were mounted onto a stage and then coated with gold for 2 min by EM350 sputter. Images were acquired *via* a JEOL-1530 Thermally-Assisted Field Emission (TFE) Scanning Electron Microscope (SEM) at 5 kV at various resolving powers.

Coherent anti-Stokes Raman scattering (CARS) microscopy

A mode-locked Nd:VAN laser (High Q Laser (US), Inc) is used to generate 7 ps, 76 MHz pulse trains of both 1064 and 532 nm laser beam. The 1064 nm beam is used directly as the Stokes beam. The 532 nm beam pumps an optical parametric oscillator (OPO) (Levante Emerald, APE-Berlin) to generate the CARS pump beam. The pump beam is tuned to 910 nm to effectively detect the 1600 cm^{-1} Raman band. Colinear and temporally overlapped pump and Stokes beam are focused onto the sample. The excitation power after objective is kept at ~ 350 mW for the pump and ~ 150 mW for the Stokes beam. The *Populus* stem is cut into ~ 20 μm by rotary microtome (Leica RM2255, Leica Microsystems Inc) embedding processes and the slice is spread out in between two coverslips. CARS image of lignin in the slice is obtained at 1600 cm^{-1} . The focused beams are raster scanned over the sample. The anti-Stokes light is collected from the Epi-direction and filtered by a clean-up filter 800/40 (Thorlabs).

Sample preparation of holocellulose

Sawdust samples were treated with NaClO_2 (1.30 g/1.00 g lignocellulosic dry solids) in acetic acid (375.0 mL of 0.14 M) at 70 °C for 2 h. The samples were then collected by filtration and rinsed with an excess of DI filtered water. This procedure was repeated to ensure complete removal of the lignin component.

Sample preparation for solid state nuclear magnetic resonance (NMR)

Isolated cellulose was prepared from the holocellulose sample (1.00 g) by hydrolysis for 4 h in HCl (100.0 mL of 2.5 M) at 100 °C. The isolated cellulose samples were then collected by filtration, rinsed with an excess of DI filtered water, and dried in the fume hood.

Solid-state NMR analysis

The NMR samples were prepared with ground wood or isolated cellulose added into 4-mm cylindrical ceramic MAS rotors. Solid-state NMR measurements were carried out on a Bruker Avance-400 spectrometer operating at frequencies of 100.55 MHz for ^{13}C in a Bruker double-resonance MAS probehead at spinning speeds

of 10 kHz. CP/MAS experiments utilized a 5 μs (90°) proton pulse, 1.5 ms contact pulse, 4 s recycle delay and 4–8 K scans. All spectra were recorded on pre-wet samples (30–40% water content), and the line-fitting analysis of spectra was performed using NUTS NMR Data Processing software (Acorn NMR, Inc). Error analysis was conducted by performing three individual isolations, NMR acquisitions and line-fit data processing.

Sample preparation for gel permeation chromatography (GPC)

Isolated α -cellulose was generated by first isolating holocellulose from milled biomass pulp using the above method. Isolated cellulose was prepared from the holocellulose sample (1.00 g) by extraction with a 17.5% NaOH solution (50.0 mL) at 25 °C for 30 min. 50 mL of deionized filtered water was then added to the NaOH solution. The extraction was continued with the 8.75% NaOH solution (100 mL) at 25 °C for an additional 30 min. The isolated α -cellulose samples were then collected by filtration and rinsed with 50 mL of 1% acetic acid, an excess of deionized filtered water, and air dried.

GPC analysis of cellulose

The number-average molecular weight (M_n) and weight-average molecular weight (M_w) were determined by GPC after tricarbanilation of cellulose.^{41,42} Lignin-free cellulose (15 mg) from each sample was placed in separate test tubes equipped with micro stir bars and dried overnight under vacuum at 40 °C. The test tubes were then capped with rubber septa. Anhydrous pyridine (4.0 mL) and phenyl isocyanate (0.50 mL) were added sequentially *via* syringe. The test tubes were placed in an oil bath at 70 °C and allowed to stir for 48 h. Methanol (1.0 mL) was then added to quench any remaining phenyl isocyanate. The contents of each test tube were then added dropwise to a 7 : 3 methanol:water mixture (100 mL) to promote precipitation of the derivatized cellulose. The solids were collected by filtration and then washed with methanol:water (1 \times 50 mL) followed by water (2 \times 50 mL). The derivatized cellulose was then dried overnight under vacuum at 40 °C. Prior to GPC analysis the derivatized cellulose was dissolved in THF (1 mg/mL), filtered through a 0.45 μm filter and placed in a 2 mL auto-sampler vial.

The molecular weight distributions of the cellulose tricarbanilate samples were then analyzed on an Agilent GPC SEcURITY 1200 system equipped with four Waters Styragel columns (HR1, HR2, HR4, HR5), Agilent refractive index (RI) detector and Agilent UV detector (270 nm) using THF as the mobile phase (1.0 mL/min) with injection volumes of 20 μL . A calibration curve was constructed based on eight narrow polystyrene standards ranging in molecular weight from 1.5×10^3 to 3.6×10^6 g/mol. Data collection and processing were performed using Polymer Standards Service WinGPC Unity software (Build 6807). Molecular weights (M_n and M_w) were calculated by the software relative to the universal polystyrene calibration curve. Number-average degree of polymerization (DP_n) and weight-average degree of polymerization (DP_w) were obtained by dividing M_n and M_w by 519 g/mol, the molecular weight of the tricarbanilated cellulose repeat unit. Polydispersity index (PDI) was calculated by dividing M_w by M_n . All reported values for molecular weight and degree of polymerization were the mean average of duplicate samples.

Sample preparation for ^1H - ^{13}C heteronuclear single quantum correlation (HSQC) NMR analysis

Whole cell wall and holocellulose samples were vacuum dried (at 40 °C for 48 h) and ball-milled by vibrational ball-milling for 1 h at a frequency of 25 Hz. 0.60 g mixture of 1 : 3 anhydrous pyridinium chloride- d_5 -DMSO- d_6 (99.9 atom% D) and 60 mg of sample were added to a 5 mm NMR tube, sealed after a nitrogen purge, containing a small stirrer bar. This sample tube was capped and stirred at 60 °C for 1 h. The resulting solution was clear and ready for NMR analysis after the magnet was removed and the sample tube was flushed with nitrogen and capped.

^1H - ^{13}C HSQC NMR analysis

Two-dimensional HSQC NMR correlation spectra were recorded on a Bruker DRX 500 spectrometer. The HSQC analysis was performed using a standard Bruker pulse sequence with a 90° pulse, 0.11 s acquisition time, a 1.5 s pulse delay, a $^1J_{\text{C-H}}$ of 145 Hz and acquisition of 256 data points.

Pyrolysis molecular beam mass spectrometry (py-MBMS)

The py-MBMS analyses were conducted using a pyrolysis autosampler coupled to a molecular beam mass spectrometer (MBMS) (Sykes *et al.* 2009). Ground samples (4 mg) were pyrolyzed in a furnace that was preheated to 500 °C. The molecular fragments are swept out of the autosampler furnace into the MBMS with a Helium gas stream. The gas stream expands in the first chamber to quench most intermolecular collisions. A low-energy electron beam (−17 eV) in the single quadrupole mass spectrometer produces a positive ion mass spectrum. The MBMS experiment is described in details elsewhere.^{36,43–45} Lignin contents were estimated using the summed normalized peak intensities for major peaks assigned to lignin fragments at 120, 124, 137, 138, 150, 152, 154, 164, 167, 168, 178, 180, 181, 182, 194, 208, 210.^{36,45,46} The lignin and carbohydrate values estimated by pyMBMS were verified periodically against National Institute of Standards and Technology sample (NIST 8492) by means of standard laboratory procedures and correction factors determined and applied.

Acknowledgements

This work was supported and performed as part of the Bio-Energy Science Center. The BioEnergy Science Center is a U.S. Department of Energy Bioenergy Research Center supported by the Office of Biological and Environmental Research in the DOE Office of Science. ORNL is managed by UT-Battelle, LLC, under contract DE-AC05-00OR22725 for the U.S. Department of Energy.

References

- J. Ruelle, H. Yamamoto and B. Thibaut, *Bioresources*, 2007, **2**, 235–351.
- G. Pilate, B. Chabbert, A. Yoshinaga, J. C. Leple and F. Laurans, *et al.*, *Plant Biol. Pathology*, 2004, **327**, 889–901.
- M. Wada, T. Okana, J. Sugiyama and F. Horii, *Cellulose*, 1995, **2**, 223–233.
- A. Shchukarev, B. Sundberg, E. Mellerowicz and P. Persson, *Surf. Interface Anal.*, 2002, **34**, 284–288.
- M. Yoshida, H. Ohta, H. Yamamoto and T. Okuyama, *Trees*, 2002, **16**, 457–464.
- G. Daniel, L. Filonove, A. M. Kallas and T. Teeri, *Holzforchung*, 2006, **60**, 618–624.
- M. Muller, M. Burghammer and J. Sugiyama, *Holzforchung*, 2006, **60**, 474–479.
- S. D. Mansfield, C. Mooney and J. Saddler, *Biotechnol. Prog.*, 1999, **15**, 804–815.
- R. J. Dinus, P. Payne, N. M. Sewell, V. L. Chiang and G. A. Tuskan, *Crit. Rev. Plant Sci.*, 2001, **20**, 51–59.
- N. Gierlinger and M. Schwanninger, *Plant Physiol.*, 2006, **140**, 1246–1254.
- V. Sewalt, W. Ni, H. Jung and R. Dixon, *J. Agric. Food Chem.*, 1997, **45**, 1977–1983.
- W. Grous, A. Converse and H. Grethlein, *Enzyme Microb. Technol.*, 1986, **8**, 274–280.
- M. Foston and A. J. Ragauskas, *Energy Fuels*, 2010, **24**, 5677–5685.
- L. T. Fan, Y. Lee and D. Beardmore, *Biotechnol. Bioeng.*, 1980, **22**, 177–199.
- Y. P. Zhang and L. Lynd, *Biotechnol. Bioeng.*, 2004, **88**, 797–824.
- Y. Zeng, B. Saar, M. G. Friedrich, F. Chen and Y. Ding, *et al.*, *BioEnergy Res.*, 2010, **3**, 272–277.
- B. G. Saar, Y. Zeng, C. W. Freudiger and Y. Ding, *et al.*, *Angew. Chem., Int. Ed.*, 2010, **49**, 5476–5479.
- M. Fujii, J. Azuma, F. Tanka, A. Kato and F. Koshijima, *Wood Res.*, 1982, **68**, 8–21.
- A. Sluiter and J. Sluiter *Determination of Starch in Solid Biomass Samples by HPLC* National Renewable Energy Laboratory Golden, Colorado 2008.
- S. D. Mansfield and R. Meder, *Cellulose*, 2003, **10**, 159–169.
- Y. P. u, C. Ziemer and A. J. Ragauskas, *Carbohydr. Res.*, 2006, **341**, 591–597.
- K. Wickholm, P. T. Larsson and T. Iversen, *Carbohydr. Res.*, 1998, **312**, 123–129.
- M. Foston and A. J. Ragauskas, *Biomass Bioenergy*, 2010, **34**, 1885–1895.
- L. Heux, E. Dinand and M. R. Vignon, *Carbohydr. Polym.*, 1999, **40**, 115–124.
- S. Jacobsen and C. Wyman, *Appl. Biochem. Biotechnol.*, 2000, **84–86**, 81–96.
- N. Mosier, C. Wyman, B. Dale, R. Elander, Y. Lee and M. Holtzapple, *et al.*, *Bioresour. Technol.*, 2005, **96**, 673–686.
- M. J. Negro, P. Manzanares, J. M. Oliva, I. Ballesteros and M. Ballesteros, *Biomass Bioenergy*, 2003, **25**, 301–308.
- F. Chen and R. Dixon, *Nat. Biotechnol.*, 2007, **25**, 759.
- W. Hu, S. Harding, J. Lung, J. Popko and J. Ralph, *et al.*, *Nat. Biotechnol.*, 1999, **17**, 808–812.
- D. J. Yelle, J. Ralph and C. R. Frihart, *Magn. Reson. Chem.*, 2008, **46**, 508.
- H. Kim, J. Ralph and T. Akiyama, *BioEnergy Res.*, 2008, **1**, 56.
- H. Kim and J. Ralph, *Org. Biomol. Chem.*, 2010, **8**, 576.
- W. Mander, *Holzforchung*, 1987, **41**, 13–18.
- Y. Wang, J. Gril, B. Clair, K. Minato and J. Sugiyama, *Trees*, 2010, **24**, 541–549.
- Y. Pu, F. Chen, A. Ziebell, B. Davison and A. J. Ragauskas, *BioEnergy Res.*, 2009, **2**, 198–208.
- S. Kelley, R. Rowell, M. Davis, C. Jurich and R. Ibac, *Biomass Bioenergy*, 2004, **27**, 77–88.
- E. N. Tokareva, P. Fardim, A. V. Pranovich and H. P. Fagerholm, *et al.*, *Appl. Surf. Sci.*, 2007, **253**, 7569–7577.
- T. K. Ghose, *Pure Appl. Chem.*, 1987, **59**, 257–268.
- A. G. Voragen, H. A. Schols, M. F. Leeusen, G. Beldman and F. M. Rombouts, *J. Chromatogr., A*, 1986, **370**, 113–120.
- M. Davis, *J. Wood Chem. Technol.*, 1998, **18**, 235–252.
- R. Cohen, K. A. Jensen Jr., C. J. Houtman and K. E. Hammel, *FEBS Lett.*, 2002, **531**, 483–488.
- B. F. Wood, A. H. Conner and C. G. Hill Jr, *J. Appl. Polym. Sci.*, 1986, **32**, 3703–3712.
- F. Agblevor, R. Evans and K. Johnson, *J. Anal. Appl. Pyrolysis*, 1994, **30**, 125–144.
- R. Evans and T. Milne, *Energy Fuels*, 1987, **1**, 123–137.
- D. Mann, N. Labbe, R. Sykes, K. Gracom and L. Kline, *et al.*, *BioEnergy Res.*, 2009, **2**, 246–256.
- R. Sykes, B. Kodrzycki, G. A. Tuskan, K. Foutz and M. Davis, *Wood Sci. Technol.*, 2008, **42**, 649–661.